nature nanotechnology

SUPPLEMENTARY INFORMATION

DOI: 10.1038/NNANO.2017.180

In the format provided by the authors and unedited.

Nanoscopic control and quantification of enantioselective optical forces

Yang Zhao[1,*], Amr A. E. Saleh[1,4], Marie Anne van de Haar[2], Brian Baum[1], Justin A. Briggs[3], Alice Lay[3], Olivia Alexandra Reyes-Becerra[1], and Jennifer A. Dionne[1,*]

Supplementary Note 1: Experimental setup

Supplementary Fig. 1 schematically illustrates our experimental setup. Specifically, a tunable laser source first passes through an acoustic optical modulator (AOM, Gooch & Housego AOMO 3110-191), where the modulator is driven at a frequency extracted from the shake-piezo of the AFM (Asylum Research MFP-3D Bio). The shake-piezo signal normally drives the cantilever at its natural resonance frequency based on resonance tuning; in our setup, the shake-piezo signal is instead connected to the function generator that modulates the acoustic optical modulator. The same signal is also fed to the lock-in amplifier (SRS 865, Stanford Research Systems) as the reference signal. During each measurement, the cantilever deflection signal is fed to the input of the lock-in amplifier, where a signal that matches the modulation frequency f_m is extracted as the signal that reflects the optical force.

The AFM is integrated with an inverted microscope (Zeiss, Axio Observer Z1m). The unit (AFM and optical microscope) is placed within a temperature and vibration control chamber, where a temperature stabilized heat reservoir is set to be ~5°C above room temperature with a temperature precision of 0.1°C and equilibrated with the sample for 10 hours before measurement to minimize expansion and contraction of the sample and the tip.

Laser light is guided through an optical fiber (multimode, Thorlabs) into the microscope. Circularly polarized light is created by passing a collimated beam through a linear polarizer (GT10-B Glan Taylor Polarizer, Thorlabs) and then a quarter wave plate (AQWP05M-600, Thorlabs). The laser beam is focused with a 50x objective lens (NA=0.55, Zeiss) onto the glass substrate.

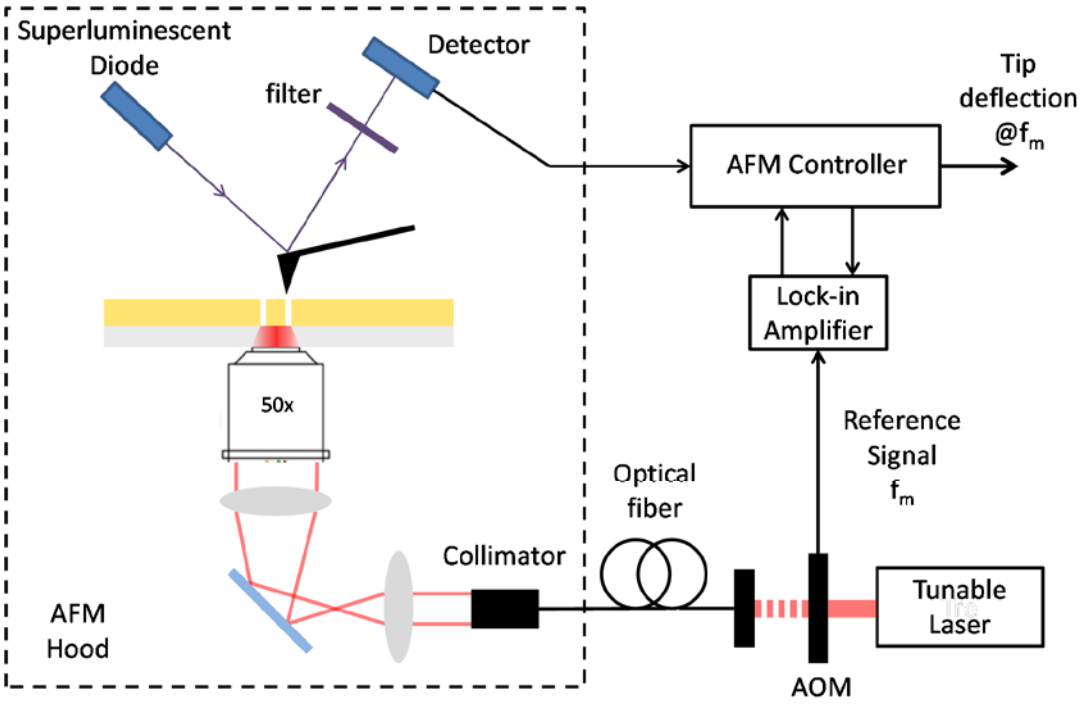

Supplementary Fig. 1| Experimental setup for optical force measurement. AOM represents acoustic optical modulator. f_m is modulation frequency of the AOM. The AFM hood indicates the temperature and vibration control chamber.

In Supplementary Fig. 2, we illustrate the force measurement scheme. As briefly mentioned in the main text, first, a non-oscillating tip approaches the sample surface, from position 1 to

position 3. Once it has reached the surface, it retracts from position 3 to 4. After reaching a constant deflection, we elevate the tip to a specific height z (position 5) and modulate the incident light through the coaxial aperture at a frequency that matches the cantilever's natural resonance but is much lower than the optical frequency of the illumination. This low-frequency modulation significantly improves the signal-to-noise ratio and enables precise measurement of the cantilever deflection for specific positions across the coaxial aperture. Note that the minimum height z where the tip is retracted to and that can be repeatedly achieved is 40 nm above the surface. This height is limited by the ambient humidity and the meniscus layer of water condensed on the surface, when the experiment is conducted in air at room temperature.

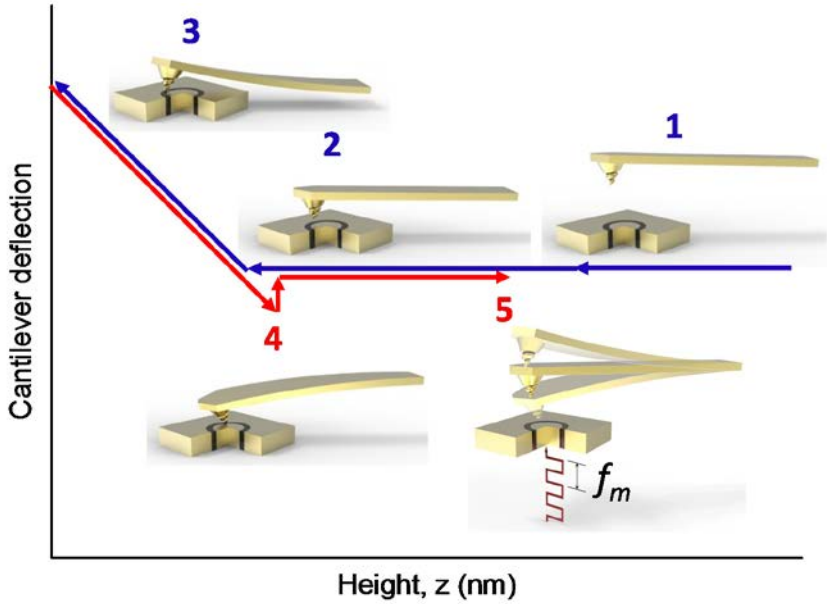

Supplementary Fig. 2| A schematic illustration of the measurement used in this study. A force-distance curve is first performed to locate the exact tip-aperture separation. When the tip retracts to a certain height, z, a gated CW laser source is turned on, with a repetition rate that matches the fundamental mechanical resonance of the cantilever.

Supplementary Note 2: Control measurement with an achiral silicon tip

We explore the polarization-dependent behavior of optical forces at various tip-aperture separations, with the incident laser fixed at the wavelength of 750 nm, which is near the resonance of the coaxial aperture. At this wavelength the ratio between the measured force and the background signal is highest, leading to the highest detection sensitivity of our setup. We first illuminate the aperture with linearly polarized light along the x direction, and use the same achiral AFM tip as in the main text (Figure 3**a**).

With x-polarized illumination, two hot spots of the local electric field intensity are expected. During this measurement, we park the tip at one of these hot spots, indicated by the black circle in Supplementary Fig. 3**a**. Supplementary Fig. 3**b** shows that a force of ~90 pN is exerted on this tip for an incident intensity of 100 μW/μm^2, at a tip-aperture separation distance of 40 nm (black curve, Supplementary Fig. 3**b**). Because of the height-precision, we are able to measure the fast-decaying nature of this optical force, by varying the separation from 40 nm up to 1000 nm. We observe an exponential decay of the force as the tip-aperture separation increases (Supplementary Fig. 3**b**). Then we rotate the incident light polarization by 90 degrees (now along the y direction), and measure the optical force at the same location of the aperture. In this case, the magnitude of the force is ~45 pN at a tip-aperture separation of 40 nm, which is 50% less compared to what is measured with the x-polarized illumination at the same location. The optical force also decays much slower compared to the x-polarized case. The linear polarization-dependent force is expected from numerical simulations of the local fields, where the maximum force tracks the hot-spots of the local electric field. Such trends are consistent with the qualitative trends seen in several prior studies, where the field distribution can be measured with near-field scanning microscopy[1-5].

To measure the linear polarization-dependent force with the chiral tip, we separately illuminate the nanoaperture with x- and y-linearly polarized light. We park the chiral tip at the same locations as indicated by Supplementary Fig. 3**a** for both x- and y- linearly polarized illumination. As expected, the force follows a similar trend to that measured on the achiral tip with linear polarizations, i.e. exponential decay as the tip-aperture separation increases. The force magnitudes are higher in this scenario, because the higher electric polarizability of gold contributes to the overall force. We discuss more control experiments to investigate this higher force magnitude in the following section.

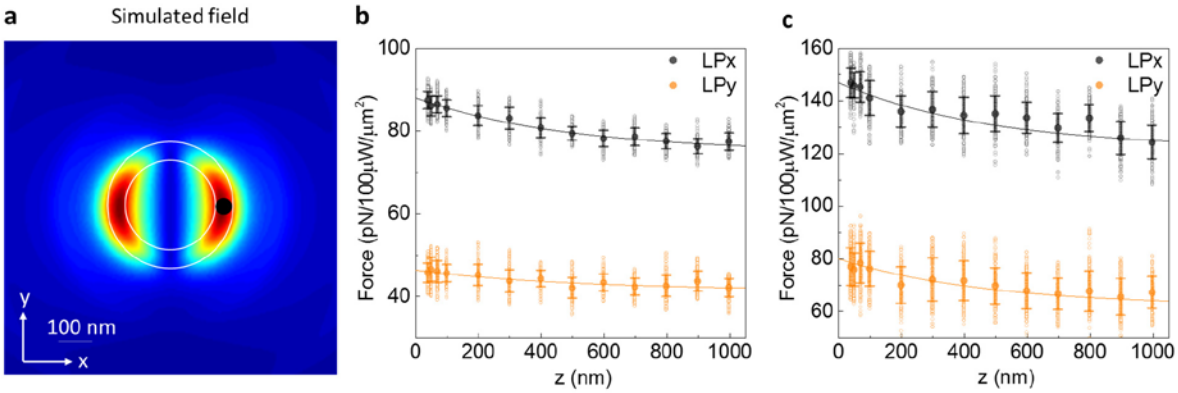

Supplementary Fig. 3| Optical force measurement with an achiral silicon probe in comparison to the chiral probe with linearly polarized illumination. a, Simulated electric field profile on the transmission side of the coaxial aperture, illuminated with x-polarized light, with the black dot indicating the tip position during the measurement. **b**, measured optical forces with x- (black dots) and y- (orange dots) linearly polarized illumination with the achiral silicon probe. **c**, measured optical forces with x- (black dots) and y- (orange dots) linearly polarized illumination with the chiral probe.

Supplementary Note 3: Control measurement with an achiral gold coated silicon tip

In addition to the control experiment with an achiral silicon probe (Figure 3**a** in the main text, and Supplementary Fig. 3), we also perform a second control experiment with an achiral gold-coated silicon tip (PPP-FMAu, Nanosensors). This probe has the same shape and similar spring constant (1.23 nN/nm) as the silicon probe used in the control experiment, but it has an additional 35 nm gold coating on both the tip side and the back reflection side. We repeat the same optical force measurements shown in Supplementary Fig. 3 and Figure 3 by first illuminating the aperture with linear polarizations along the x and y directions, and then left- and right-handed circular polarizations.

We show in Supplementary Fig. 4**a** that with x-polarized light the exponential decay is similar to both the achiral silicon probe and the chiral probe (Supplementary Fig. 3). The values of the measured forces closely match the chiral probe (Supplementary Fig. 3**c**) due to the presence of gold, which possesses a high electric polarizability. When illuminating the aperture with linear polarization along the y direction, we measure ~ 80 pN forces with 100 μW/μm^2 illumination intensity.

In Supplementary Fig. 4**b**, we show the measured enantioselective forces with this achiral gold probe with circularly polarized illumination. The solid curves are exponential decay fits, and serve as a guide-to-the-eye. As expected, the two curves closely follow each other with a small difference of ~3 pN due to the inherent structural asymmetry of the probe. For a better comparison, we reproduce the results measured with the chiral probe, and display that here in Supplementary Fig. 4**c** and 4**d**. Note that the standard deviation for this set of control measurement is slightly larger compared to the ones with the achiral silicon probe and the chiral probe in Figure 3. This difference can be attributed to three aspects: fluctuation in the power of

the laser source, local humidity, and local heating of the gold probe. We calibrate the thermal fluctuation in this set of control experiments: the x drift is 378 pm per minute and the y drift is 1.1 nm per minute. In contrast, for the experiment in Figure 3, the x drift is 354 pm per minute and y drift is 360 pm per minute.

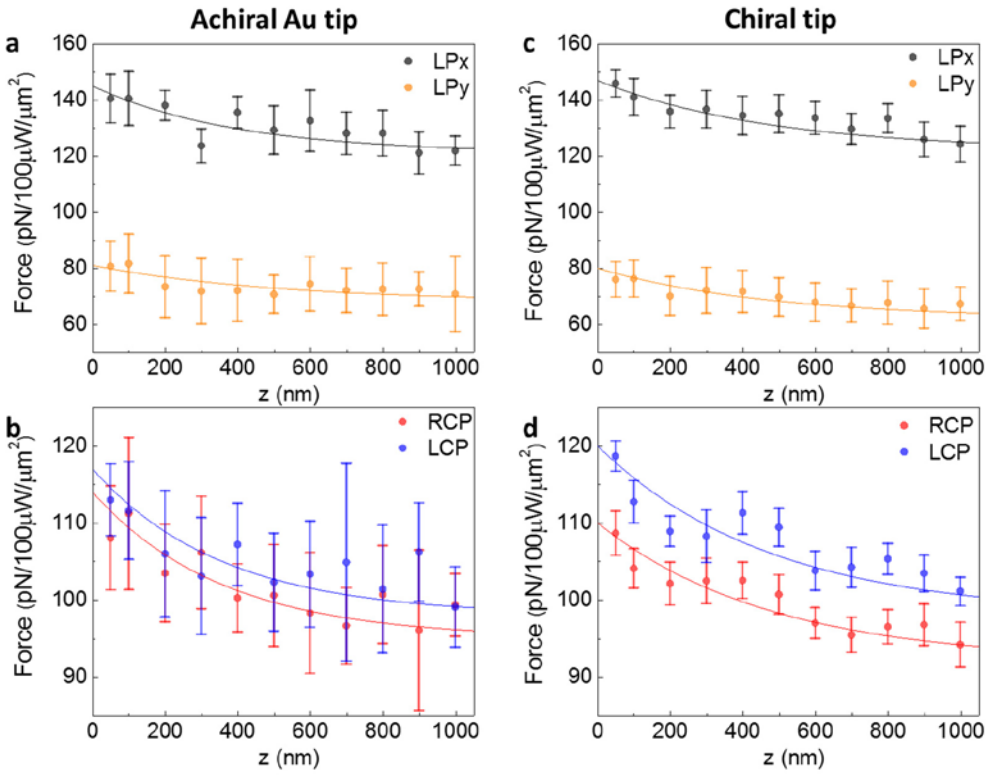

Supplementary Fig. 4| Optical force measurement with an achiral gold probe in comparison to chiral probe. a, measured optical forces with linearly polarized illumination along x (black dots), and y (orange dots) directions. **b**, measured optical forces with left-handed (blue dots), and right-handed (red dots) circularly polarized illumination. For comparison, we display again here the measured optical forces with chiral tip for x- (black dots) and y-linearly (orange dots), left- (blue dots) and right-handed circularly (red dots) polarized illumination, in panels (**c**) and (**d**) respectively.

Supplementary Note 4: Control measurement with a chiral tip of left-handedness made of non-plasmonic materials

Our chiral tip shown in Figure 3 in the main text is not on its plasmonic resonance given the pitch of the spiral; the resonances of the chiral structure are in the infrared region (peak at 1800 nm and 2500 nm, respectively). To help exclude plasmonic heating from the tip, we conducted additional experimental studies on a non-plasmonic chiral tip. We fabricated such chiral tip by depositing Pt on a silicon tip (PPP-FM, nanosensors). The silicon tip has the same shape and spring constant as we used in our control experiments in Supplementary Note 2 above. The non-plasmonic chiral tip is shown in Supplementary Fig. 5 below. It is seen that the Pt chiral tip also measures enantioselective forces with a similar trend in their decay. These results are qualitatively comparable to the ones that we measured with the gold chiral tip, indicating that the plasmonic response of the chiral tip doesn't play a significant role. We can thus largely rule out thermal contributions.

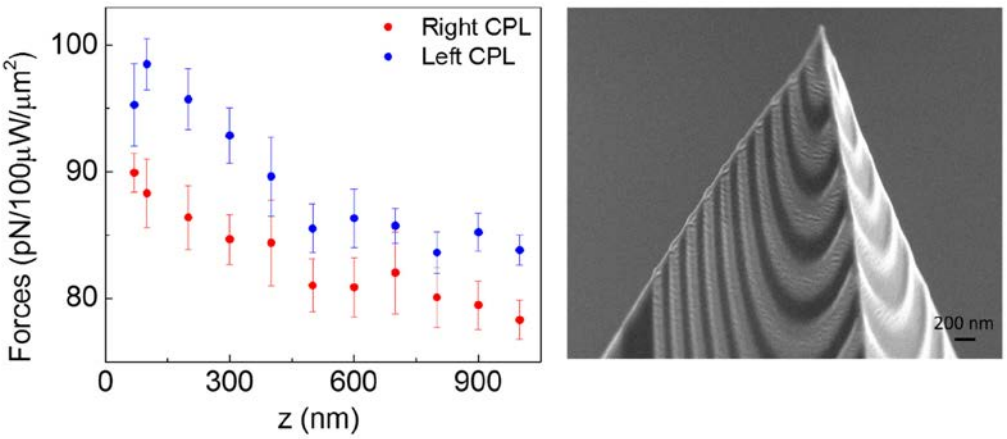

Supplementary Fig. 5| Control experiment using coaxial aperture with chiral tip made by depositing a Pt spiral pattern on similar silicon AFM tips.

Supplementary Note 5: Control measurement with a chiral tip of right-handedness (R)

To understand how the chirality of the tip plays a key role in the measured enantioselective forces, we performed additional experiments. We made another chiral tip that has opposite handedness compared to the one shown in Figure 3 in the main text. This new chiral tip is fabricated on the same type of tip (PPP-FMAu, Nanosensors) with comparable dimension of the chiral nano-structure as we show in Figure 3 in the main text, but with a spiral of opposite rotation as shown in Supplementary Fig. 6**a**, now right-handed (R). We again illuminate this right-handed chiral tip with left- and right- CPL respectively.

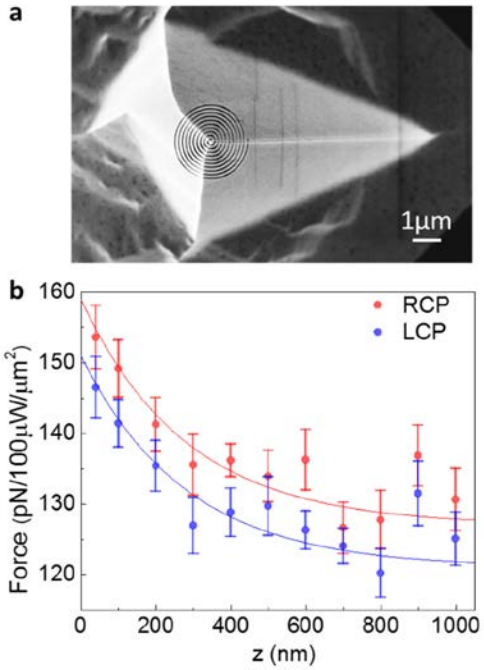

Supplementary Fig. 6| Optical force measurement with chiral probe of right-handedness (R). **a**, Scanning electron microscope (SEM) image of the chiral probe with an opposite handedness (R) compared to Figure 3 in the main text (L). **b**, Measured optical forces with left- (blue dots), and right- (red dots) CPL illuminations.

In Supplementary Fig. 6**b**, we show that the force measured with right-CPL is larger than that measured with left-CPL, and the solid curves are exponential decay fits.

For a better visualization, we extract the enantioselective forces measured with this R-chiral probe, and re-displayed the enantioselective forces measured with the L-chiral probe and the achiral probe simultaneously in Supplementary Fig. 7 (the L-chiral probe and achiral probe are re-displayed from Figure 3**e** in the main text). Note that the enantioselective forces are defined as the difference in optical forces by subtracting the force measured with right-CPL illumination from left-CPL illumination.

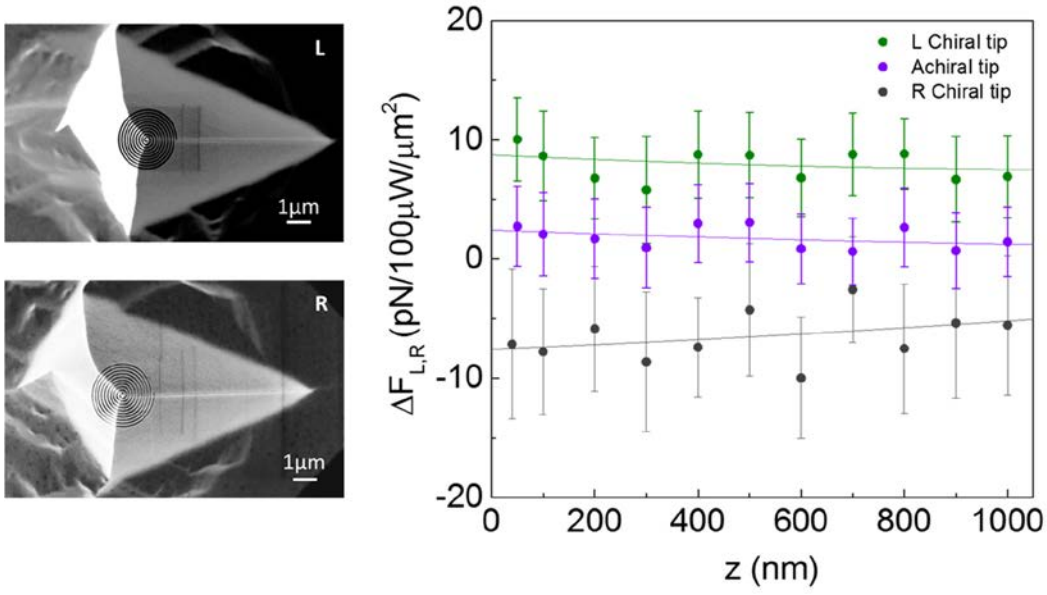

Supplementary Fig. 7| Enantioselective optical forces measured with tips patterned with L- and R- chiral spirals, and an achiral tip as a function of tip-aperture separation (z). The solid lines are polynomial fitting to the data. The SEM images on the left are top-views of the L- and R- chiral spiral patterned tips.

Supplementary Fig. 7 shows that the enantioselective chiral tips measure opposite

enantioselective optical forces ($\Delta F_{L,R}$). Because the achiral tip poses slight positive enantioselective forces as also shown in Figure 3**e**, the newly measured enantioselective force is slightly weaker. These results help prove that the measured enantioselective forces arise from chirality.

Supplementary Note 6: Control measurement with the above chiral tip (R-chiral) without passing through the coaxial aperture

We also performed additional control experiments to directly measure the chiral forces upon direct circularly polarized illumination through the glass substrate on the R-chiral tip, without passing through the nanoaperture (Supplementary Fig. 8).

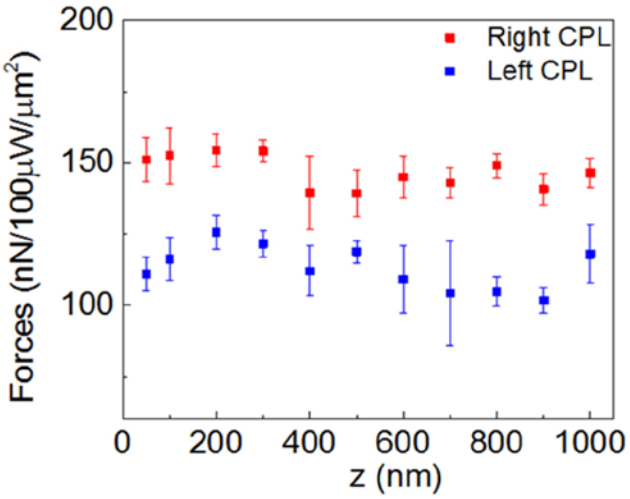

Supplementary Fig. 8| Control experiment without the coaxial nanoaperture. Optical forces with the same chiral tip shown in Supplementary Fig. 5**a**, but measured with directly illuminating through the class substrate without passing through the coaxial aperture.

Supplementary Fig. 8 shows that without the nanoaperture, the decay rate of the measured forces as a function of tip-aperture distance (z) is much slower, compared to the case measured with the apertures shown in Figure 3 in the main text. The reduced decay rate here is attributed to the much slower changing gradient of a focused beam in air, compared with that transmitted through a nanoaperture. The oscillation of the measured force is present in both scenarios (with or without nanoapertures), which corresponds to the fabry-perot resonances of the cavity formed between the tip and the aperture surface.

The measured forces without passing through the nanoaperture are in the range of nanoNewton compared to the picoNewton forces with the nanoaperture. Please note that all measured forces are normalized to the same *incident* illumination intensity. The transmission of the nanoaperture is ≤10% compared to the transmission through the glass substrate; therefore the trapping light intensity is more than 10 times stronger without the coaxial nanoaperture. Additionally, without passing through the nanoaperture, the entire chiral structure on the tip (in the dimension up to a few microns) sees the circularly polarized field. Because the measured optical forces are proportional to the volume of the tip as well as the transmitted intensity, the higher magnitude forces from this control experiment without the coax are expected. By taking into account the stronger trapping light and the size difference of the tip involved in the force measurement, we expect the measured forces to be scaled up by at least 10^4 times on such micron-sized chiral specimen. It is seen that the measured forces increases only ~10^3 times, pointing to the enhancement effect from our nanoaperture. Lastly, in the scenario with the nanoaperture, we also enhanced the resolution of the trapping potential because the width of the trapping potential is directly associated with the size of the focused beam, which is ~27 um in diameter without the coaxial aperture versus ~60 nm (in terms of the width of the dielectric channel) with the aperture.

Supplementary Note 7: Measurement of the direction of optical forces

To verify the direction of our optical force - i.e. is the force towards the +z direction (pushing force) or the –z direction (pulling force) - we perform a control experiment, where a tipless cantilever is used to detect the direction of this force. In a tapping mode measurement, during which the cantilever is oscillating at its natural frequency, the phase change due to external force is directly related to the direction of the force. A positive change of the phase indicates an attractive force (or a pulling force), while a negative change of the phase indicates a repulsive force (or a pushing force). We show in Supplementary Fig. 9 that when the laser is on, the phase of the cantilever oscillation has a positive change, which indicates that our optical force is a pulling force. The tipless silicon cantilever (Nanosensors, TL-CONT) has a spring constant of 0.647 nN/nm.

As we have shown in Figure 4**a** and **b**, similar experiment is conducted to obtain the map of the forces with left- and right- CPL illuminations to the plasmonic tweezer. During the force mapping, the tip first locates the surface, then elevates to a height of 40 nm. The oscillation of the cantilever is then driven by the modulated light. In Figure 4, we extract the phase of these measurements and normalize to the background signal, where the background signal is defined as the signal measured on the gold surface. From these measurements, Figure 4 shows the signal to background is larger than 1, indicating an increment of phase due to the measured optical forces. The increment of phase corresponds to a pulling/attractive force (i.e. the total force is pointing towards the nanoaperture) for both left- and right- CPL illuminations.

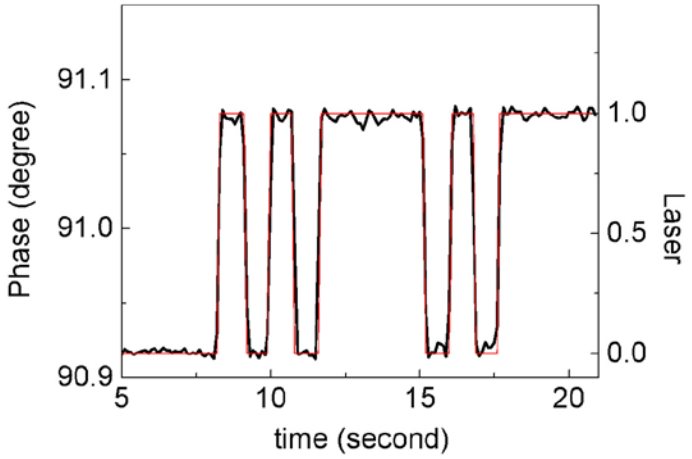

Supplementary Fig. 9| Phase change in oscillating mode (AC mode) to measure the direction of optical forces. The black curve is the measured phases, the red curve is a guide-to-the-eye indicating the on/off status of the laser.

Supplementary Note 8: Theoretical analysis of the enantioselective optical forces

In the following section, we describe how we calculate the enantioselective optical forces based on a semi-analytical approach proposed in reference 6.

Optical forces originate from the polarizability of a specimen. When illuminated by light, charges respond to the local electric field and creates dipole moments. In general, optical forces can be described as[7]:

$$\boldsymbol{F} = Re\{(\boldsymbol{p}\cdot\nabla)\boldsymbol{E} + (\boldsymbol{m}\cdot\nabla)\boldsymbol{H} + \mu_0\dot{\boldsymbol{p}}\times\boldsymbol{H} - \varepsilon_0\dot{\boldsymbol{m}}\times\boldsymbol{E}\}, \quad (1)$$

where $\boldsymbol{E}$ and $\boldsymbol{H}$ are the electric and magnetic fields, and μ_0 and ε_0 are the permeability and permittivity of vacuum, and $\boldsymbol{p}$ and $\boldsymbol{m}$ are the electric and magnetic dipole moments that contain

the material properties of the specimen. Most materials have negligible magnetic permeability at optical frequencies (i.e. $\mu_r = 1$), and weakly respond to magnetic fields; therefore optical force is normally considered to scale with the electric polarizability of the specimen and the gradient of local electric field intensity[8].

When a specimen is chiral, the local electric (magnetic) field can induce a magnetic (electric) dipole moment; this relation is described by the electromagnetic polarizability (α_{em}) of the specimen, which is directly proportional to how 'chiral' it is[9]. As we have shown in reference 6, for chiral specimens, transverse optical forces (forces in the x-y plane) through a plasmonic tweezer can be modified as:

$$\boldsymbol{F}_{tr} \approx \frac{\mathrm{Re}(\alpha_{ee})}{4}\nabla|\boldsymbol{E}|^2 + Im(\alpha_{em})\frac{1}{2}\nabla Im(\boldsymbol{E}\cdot\boldsymbol{H}^*), \quad (2)$$

where α_{ee} is the electric polarizability, and α_{em} is the electromagnetic polarizability. The first term in equation (2) is the conventional gradient optical force, while the second term is the gradient chiral force. For chiral specimens with opposite handedness (enantiomers), the gradient chiral force changes sign, and it also scales with the gradient of the optical chirality density of the local field, $\nabla(Im(\boldsymbol{E}\cdot\boldsymbol{H}^*))$ [ref 10].

8.1 Calculated transverse optical forces with circularly polarized light

We first simulate the electric and magnetic fields using a commercially available software based on the finite-difference time-domain method (FDTD, Lumerical). We record the fields at heights from 30 nm up to 60 nm above the aperture for proof of principle. These separations match our

experimental condition in Figure 3.

We use an estimated particle size to simulate the tip apex, which corresponds to the radius of curvature of the apex (~38 nm). To simulate the chiral tip, we use the material properties of gold[11] and silicon with an effective medium theory at the wavelength of 750 nm, and with a chirality parameter of -1. To demonstrate how the transverse forces change with tip-aperture separation, we integrate the transverse forces along the aperture to obtain the trapping potential (Supplementary Fig. 10). Note that we plot the negative of the trapping potentials as shown in Figure 3f in the main text. As seen in Supplementary Fig. 10**a**, when illuminating the aperture with left-handed circularly polarized light, the trapping potential on the chiral tip decays as the tip-aperture separation increases; when illuminating the aperture with right-handed circularly polarized light, the chiral tip feels a trapping *barrier*, which also decays as the separation increases. This result matches our experimental observations (main text, Figure 3f), which are reproduced here in Supplementary Fig. 10**b** and Supplementary Fig. 10**c**. Specifically, to emphasize the contribution from the gradient *chiral* force that confirms the trends in the simulated trapping potential, we remove the conventional gradient force (term 1 in equation (2)). To do so, we fit the transverse forces with exponential decays for tip-aperture separation (z) larger than 100 nm (black curve in Supplementary Fig. 10**b**); then in Supplementary Fig. 10**c**, we have removed this gradient force contribution from the transverse forces.

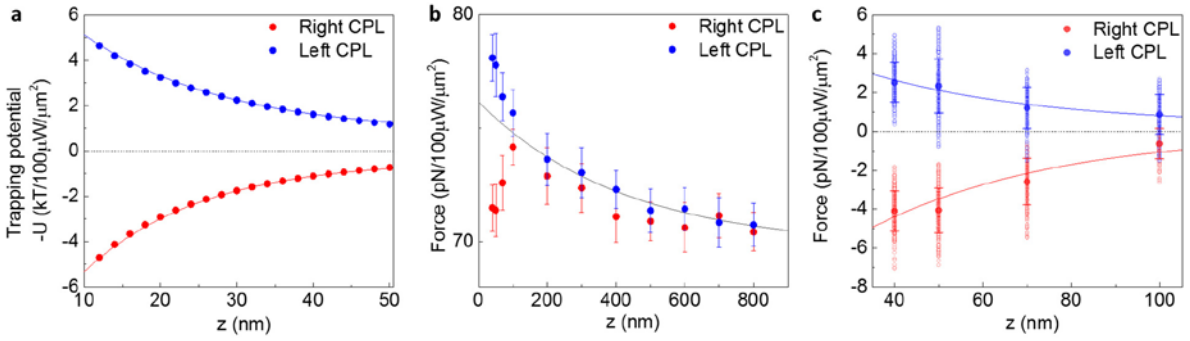

Supplementary Fig. 10| Simulated transverse trapping potentials/barriers that demonstrate the trends in the optical forces as a function of tip-aperture separation. a, simulated transverse trapping potential exerted from the coaxial aperture on a chiral nanoparticle with sizes comparable to the tip radius to illustrate the trends in the transverse forces. **b**, measured transverse forces with larger tip-aperture separations. The black curve is an exponential decay, fit to tip-aperture separation larger than 100 nm. **c**, measured transverse forces after correcting the gradient force component.

8.2 Simulation of anisotropy and perturbation of the tip to explain the decay rate

In the experiment, the AFM tip has a tetrahedral shape at the apex; but our above simulation only takes into account a spherical shaped tip as a model, therefore anisotropy may also play a role. To investigate how anisotropy affects the enantioselective forces, we introduce anisotropy in the x and z directions of the tip in the numerical model, respectively, as shown in Supplementary Fig. 11. In this simulation, we assume two types of linear anisotropy of the tip as $\alpha_{ee} = \alpha[2,0,0;\ 0,1,0;\ 0,0,1]$ as shown in Supplementary Fig. 11**b**, and $\alpha_{ee} = \alpha[1,0,0;\ 0,1,0;\ 0,0,2]$ as shown in Supplementary Fig. 11**c**. It is seen that the anisotropy can largely affect the magnitude of the forces, but not the decay rate of the associated potentials.

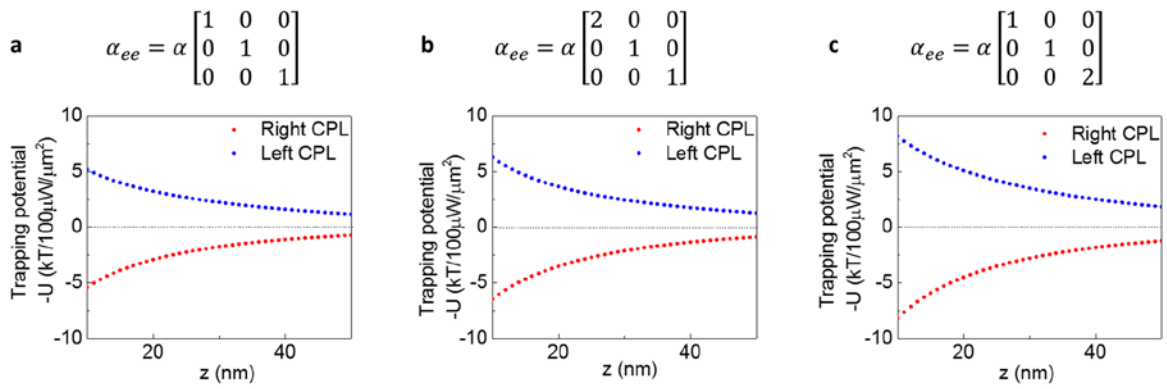

Supplementary Fig. 11| Calculated trapping potentials as a function of tip-aperture separation when considering the anisotropy of the tip. a, The tip is considered as an isotropic sphere; **b**, the tip is considered as an anisotropic sphere with anisotropy along the x direction; and **c**, the tip is anisotropic along the z direction.

The slight discrepancy in the decay rate is caused by the perturbation of the tip. In our simulation, we used a semi-analytical approach. As we described in Section 8.1 above, we extract field distribution based on FDTD numerical simulations and simulate the forces using a spherical particle. However, in the experiment, the tip will slightly perturb the field, especially when the tip-aperture separation is small.

To take into account this perturbation, we introduce a chiral scatter with the comparable size of the tip at the transmission side of the nanoaperture. In this analysis, we assume the local field is a combination of the initial illuminated plane wave and the scattered field from the scatter at each height (z=40, 50, 70, and 100 nm), respectively. With the scatter taken into account, we recalculated the trapping potentials as a function of tip-aperture separation from 40 to 100 nm that match our experimental setups, as shown in Supplementary Fig. 12 below.

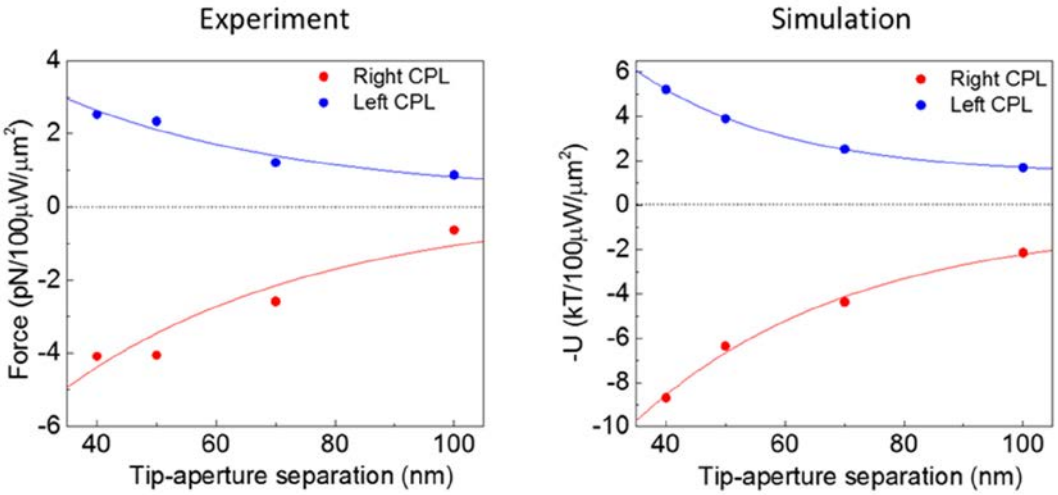

Supplementary Fig. 12| Calculated trapping potentials as a function of tip-aperture separation when the perturbation of the tip is considered.

Supplementary Fig. 12 shows a better match between the simulated and the experimental data in terms of the decay rate. For example, the exponential decay factor with left-CPL illumination is 42.2 in the experiment versus 35.8 in the simulation. Our results show that the decay of the forces does depend on feedback between the tip and the aperture. On a side note, torque may also contribute to the measured forces, which is not considered in our simulation.

8.3 Simulation of the induced displacement current inside the chiral tip

When illuminated with circularly polarized light, the coaxial nanoaperture provides strong local chirality density, which induces displacement current that propagates along the chiral structure of the tip. The consequently induced magnetic moment in the tip interacts with the electric and magnetic fields, which gives rise to the overall enantioselective optical forces[6,7,9]. An achiral

structure doesn't induce magnetic moment, given that the tips are made of non-magnetic materials. Therefore the induced displacement current, which is associated with the chirality of the tip, is the fundamental cause of the different enantioselective optical forces that we measured.

To demonstrate the induced displacement current, we conducted theoretical studies using COMSOL Multiphysics. Our simulations are based on the dimensions and materials used in our experiment for both the nanoaperture and the tip. They show that when the same chiral tip is illuminated with left- and right- circularly polarized light (CPL) respectively, the induced displacement currents point in opposite directions.

More specifically, Supplementary Fig. 13**a** shows the chiral tip illuminated with left-CPL. The color map indicates the intensity of the displacement current, as well as the direction of the out-of-plane (y) component of the current; the arrows indicate the directions of the in-plane (x, z) components of the displacement current. It is seen that by comparing left-CPL illumination with right-CPL illumination (Supplementary Fig. 13**b**), the displacement current is reversed, especially close to the tip. The reversed current corresponds to the change of sign in the second term of equation (2).

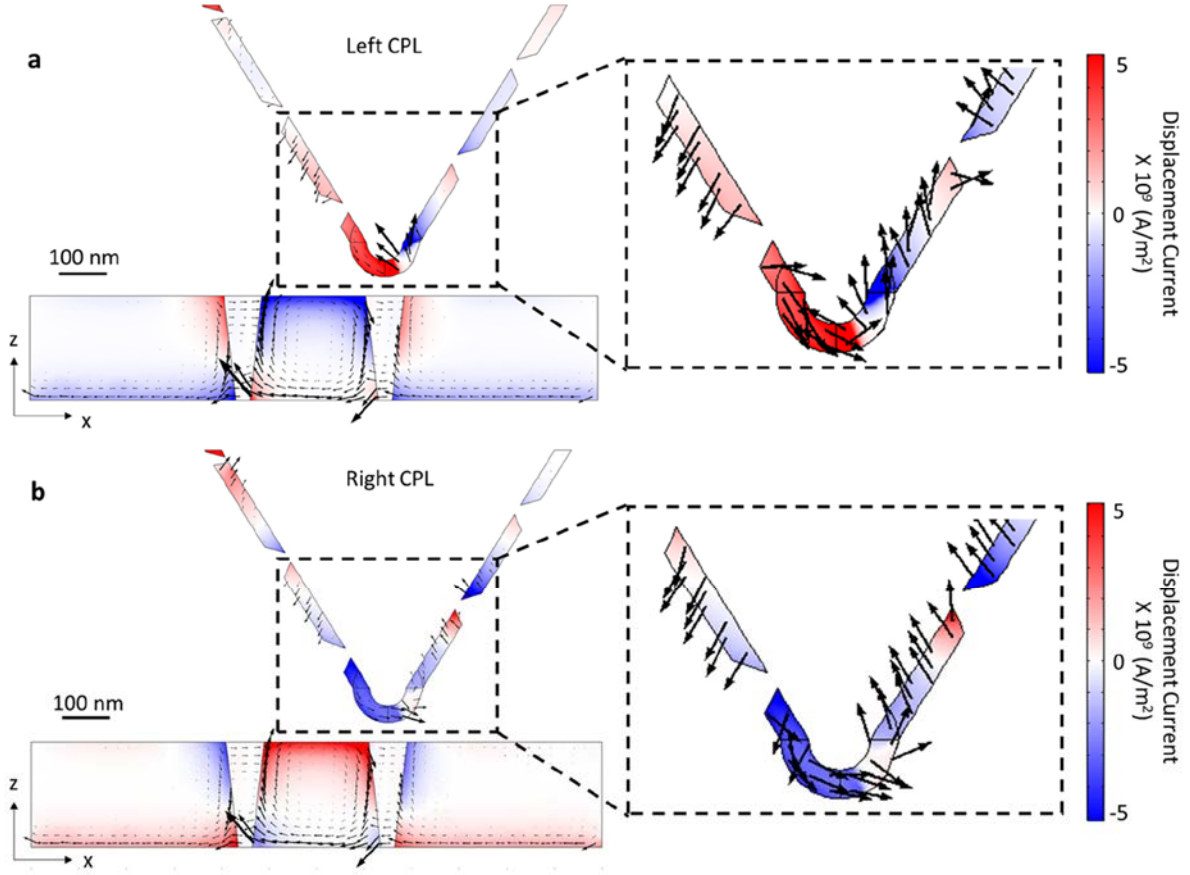

Supplementary Fig. 13| Simulated displacement current that gives rise to the enantioselective optical forces. Cross-sectional views of the displacement currents in the x-z plane, with **a**, the nanoaperture illuminated with left CPL; and **b**, the nanoaperture illuminated with right CPL. The dotted square in both panels highlights the zoomed-in displacement current near the chiral tip, where the arrows show the direction of the displacement current with the length normalized.

Supplementary References

1. Schnell, M. et al. Real-space mapping of the chiral near-field distributions in spiral antennas and planar metasurfaces. *Nano Letters* **16**, 663-670 (2016).
2. Kohoutek, J. et al. Opto-mechanical force mapping of deep subwavelength plasmonic modes. *Nano Letters* **11**, 3378-3382 (2011).
3. Khanikaev, A.B. et al. Experimental demonstration of the microscopic origin of circular dichroism in two-dimensional metamaterials. *Nature communications* **7**, 12045 (2016).
4. Huang, F., Tamma, V.A., Mardy, Z., Burdett, J. & Wickramasinghe, H.K. Imaging nanoscale electromagnetic near-field distributions using optical forces. *Scientific Reports* **5**, 10610 (2015).
5. Deutsch, B., Hillenbrand, R. & Novotny, L. Visualizing the optical interaction tensor of a gold nanoparticle pair. *Nano Letters* **10**, 652-656 (2010).
6. Zhao, Y., Saleh, A.A.E. & Dionne, J.A. Enantioselective optical trapping of chiral nanoparticles with plasmonic tweezers. *ACS Photonics* **3**, 304-309 (2016).
7. Canaguier-Durand, A., Hutchison, J.A., Genet, C. & Ebbesen, T.W. Mechanical separation of chiral dipoles by chiral light. *New Journal of Physics* **15**, 123037 (2013).
8. Ashkin, A., Dziedzic, J.M., Bjorkholm, J.E. & Chu, S. Observation of a single-beam gradient force optical trap for dielectric particles. *Optics Letters* **11**, 288-290 (1986).
9. Bekshaev, A.Y. Subwavelength particles in an inhomogeneous light field: optical forces associated with the spin and orbital energy flows. *Journal of Optics* **15**, 044004 (2013).
10. Tang, Y. & Cohen, A.E. Enhanced enantioselectivity in excitation of chiral molecules by superchiral light. *Science* **332**, 333-336 (2011).
11. Johnson, P.B. & Christy, R.W. Optical constants of the noble metals. *Physical Review B* **6**, 4370-4379 (1972).